Molecular Polarizability in Open Ensemble Simulations of Aqueous Nanoconfinements under Electric Field

F. Moucka[a,b], S. Zamfir[a], D. Bratko[a,*], A. Luzar[a]

Department of Chemistry, Virginia Commonwealth University, Richmond, VA 23221, USA[a] and Faculty of Science, J.E. Purkinje University, 400 96 Ústí nad Labem, Czech Republic[b]

Mar 23, 2019

ABSTRACT

Molecular polarization at aqueous interfaces involves fast degrees of freedom that are often averaged-out in atomistic-modeling approaches. The resulting effective interactions depend on specific environment, making explicit account of molecular polarizability particularly important in solutions with pronounced anisotropic perturbations, including solid/liquid interfaces and external fields. Our work concerns polarizability effects in nanoscale confinements under electric field, open to unperturbed bulk environment. We model aqueous molecules and ions in hydrophobic pores using the gaussian-charge-on-spring BK3-AH representation. This involves nontrivial methodology developments in Expanded Ensemble Monte Carlo simulations for open systems with long-ranged multibody interactions and necessitates further improvements for efficient modeling of polarizable ions. Structural differences between fixed-charge and polarizable models were captured in Molecular Dynamics simulations for a set of closed systems. Our open ensemble results with BK3 model in neat-aqueous systems capture the ~10% reduction of molecular dipoles within the surface layer near the hydrophobic pore walls in analogy to reported quantum mechanical calculations at water/vapor interfaces. The polarizability affects the interfacial dielectric behavior and weakens the electric-field dependence of water absorption at pragmatically relevant porosities. We observe moderate changes in thermodynamic properties and atom and charged-site spatial distributions, the Gaussian distribution of mobile charges on water and ions in the polarizable model shifts the density amplitudes and blurs the charge-layering effects associated with increased ion absorption. The use of polarizable force field indicates an enhanced response of interfacial ion distributions to applied electric field, a feature potentially important for in silico modelling of electric double layer capacitors.

I. INTRODUCTION

Avoiding the complexities associated with computational treatments of multibody effects, aqueous solutions are often modelled using effective, pairwise-additive solute and solvent interactions. At this level of approximation, molecular polarizability is accounted for only implicitly through model parameterization. While often enabling a reasonable description of liquid and solution properties[1,2], the additivity approximation becomes less accurate in the presence of spatial anisotropies, e.g. at interfaces[3], as well as upon addition of ionic species[4] or external electric fields[5]. Confined electrolytes, in or out of applied electric fields, play an essential role in biophysics and numerous technologies including energy applications. The need for better understanding and control of confined electrolytes, and their equilibrium with the environment, motivate developments of advanced models and pertinent sampling ~~techniques~~ algorithms. Incorporation of molecular polarizabilities is among main potential improvements, however, it represents considerable challenges in open systems with fluctuating density or composition. Grand Canonical (GC) Ensemble sampling, which provides a natural route to equilibrium properties of open systems, typically relies on Monte Carlo (MC) techniques whose adaptations to multi-body interactions are more complex than in Molecular Dynamics simulations.[5,6] Only a limited number of open (Grand Canonical Monte Carlo (GCMC or Gibbs Ensemble) studies have so far addressed aqueous systems with polarizable molecular potentials, typically in bulk systems.[6-13] In the present article, we describe an application of the multiple-particle-move (MPM) implementation[14-17] of GCMC simulations to study the behavior of water in nanoconfinement equilibrated with a bulk phase reservoir. We present a comparison between a conventional nonpolarizable and polarizable model representations for field-free aqueous confinements as well as confinements spanned by electric field. In both scenarios, the confined fluid maintains equilibrium with a field-free bulk environment. We determine the uptake of model water molecules in the pores, the liquid structure in the confinement, and key thermodynamic properties, pressure and interfacial free energies. To assess the differences in the dielectric response of the two models, we monitor dipole changes of interfacial molecules in the polarizable representation and compare the average dielectric constants of the two models inside the confined liquid water film at different strengths of applied fields. We also applied the multi-particle move EE-GCMC method to address confinement/bulk NaCl solution equilibria. S*imultaneous* accounts of multi-body polarizability effects *and* computationally demanding

fractional exchanges of ions, however, render the method very compute-intense. Because of nonuniform spatial distributions, the convergence is considerable slower than in the uniform-bulk-phase simulations. Systematic calculations for polarizable-model confined electrolyte systems open to particle exchange will therefore require further code optimization. These developments will be considered in a separate study. In the present work, we provide a glimpse into molecular polarizability effects in a confined electrolyte by focusing on structural differences between the two types of force fields at ~~a~~ fixed compositions. The concentration of the confined solution used is consistent with bulk NaCl concentration of 2 mol kg^{-1} in nonpolarizable force field simulations. While the differences introduced with molecular polarizability appear moderate, a number of quantities, including the increased wetting free energy inside the pore, the reduced hydration pressure between the pore walls, and comparatively lower interfacial permittivity, can likely be associated with notable reduction of the mean molecular dipole of interfacial water in the polarizable representation.

II. MODELS AND METHODS

Simulation methodology

Models. The BK3 water FF assumes the rigid geometry of TIP4P water[18] with the gas phase experimental values of the OH bonds and HOH angle. It models the nonelectrostatic interactions by the Buckingham (EXP6) potential and the electrostatic interactions by massless Gaussian charge distributions attached by harmonic springs to the rigid backbone. An analogous representation is used to model polarizable Na^+ and Cl^- ions.[19] For further details and parameter values, see the original papers.[19,20]

Interactions with the walls of the planar nanopores are described by two different models, similarly to our previous study[4,5] where we used SPC/E[21]-Joung-Cheatham[22] FF[1-3].

The first water-wall FF, hereafter called the smooth wall (SW) model, describes the interaction of either wall (w) and the particle i at position z_i by the integrated 9-3 Lennard-Jones potential[23-27]

$$u_{iw}(z_i) = A_i\left(\frac{\sigma_{iw}}{|z_i - z_w|}\right)^9 - B_i\left(\frac{\sigma_{iw}}{|z_i - z_w|}\right)^3 \quad (1)$$

where $z_w = h / 2$ or $- h /2$, $A_i = 4\pi\rho_w\sigma_{iw}^3\varepsilon_{iw}/45$, $B_i = 15A_i/2$, ρ_w is the presumed uniform number density of interacting sites of wall material, and σ_{iw} and ε_{iw} are obtained by the Lorentz-Berthelot rules applied to the water oxygen LJ parameters σ_O and ε_O, and LJ parameters of the wall interaction sites, ε_w and σ_w. To mimic hydrocarbon walls in our previous simulations of the SPC/E FF, we used $\sigma_O = 3.166$ Å, $\varepsilon_O = 650$ J/mol [13], $\rho_w = 0.0333$ Å^{-3}, $\varepsilon_w = 0.6483$ kJ/mol, and $\sigma_w = 3.742$ Å, which secured contact angle between the SPC/E water and the modeled walls within $\sim 127 \pm 3°$. We keep identical form of oxygen-wall potential in BK3 system, however, we reparametrize the wall energy parameter, ε_w, to achieve a similar contact angle at a single wall system with both models. We thus performed a set of simulations of small droplets composed of 2028 BK3 molecules on a single smooth wall with different values of ε_w ranging from 600 to 2400 J/mol. By interpolation we obtained $\varepsilon_w = 1.09$ kJ/mol to yield a contact angle of $130 \pm 2°$; this value was hence used in our EEGCMC simulations in the confinement.

The second model of confinement walls, termed the molecular wall (MW) model, mimics the structure of butylated graphane.[28] Unlike graphene, its saturated, pure sp_3 derivative, graphane[29,30] is an insulator with negligible polarizability. Moreover, it retains its planar structure upon functionalization. We use butyl groups as our previous analysis showed these groups achieved full convergence of surface wettability with respect to chain length. Like in previous studies[4,28], the surface density of alkyl groups is ~4 nm^{-2}, close to typical density in self-assembled monolayers.[31] A snapshot of the MW confinement is shown in Fig. 1. Interactions of the MW with the solution are of Lennard-Jones type, with parametrization adopted from Jorgensen et al.[32], $\sigma_{CH3} = 3.905$ Å, $\sigma_{CH2} = 3.905$ Å, $\varepsilon_{CH2} = 0.7866$ kJ/mol, $\sigma_{CH} = 3.85$ Å, $\varepsilon_{CH} = 0.3347$ kJ/mol, $\sigma_C = 3.8$ Å, $\varepsilon_C = 0.2092$ kJ/mol, and where we used $\varepsilon_{CH3} = 0.3347$ kJ/mol resulting in contact angle $\sim 130 \pm 2°$ in our previous study of the SPC/E FF. In the BK3 system, ε_{CH3} has been adjusted by an identical factor (1.09/0.6483) as in the SW approach, i.e., we used $\varepsilon_{CH3} = 0.5628$ kJ/mol for the BK3-wall interaction in the EEGCMC simulations. As will be shown below, this value reproduces the contact angle of the SPC/E system. The separation between molecular walls was adjusted to produce the thickness of the liquid film essentially

identical to that observed in the SW model. The structure and other details of the MW model are found in refs.[4,28]

An external field is applied by imposing a fixed electric displacement fields D_z of strengths 0.00885, 0.0177, or 0.0266 C m^{-2}, which would correspond to unscreened (vacuum) fields E_o

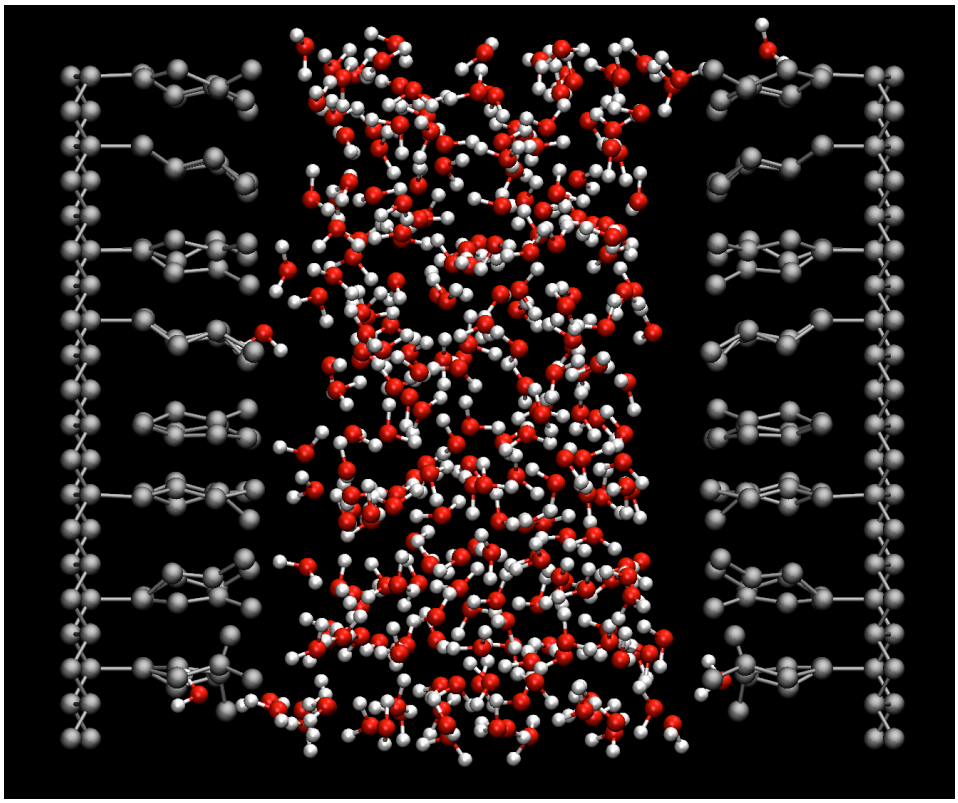

Figure 1. Snapshot of confined BK3 water film between alkyl-coated graphene plates subject to perpendicular electric field. Field E_f spanning the aqueous film (average strength ~ 0.08 V nm^{-1}) supports occasional penetrations of water molecules into the alkyl brush.

between 1-3 Vnm^{-1} . The actual (dielectrically screened) fields E_f (averaged over the width of aqueous slab) range from 0.03 to ~ 0.15 V nm^{-1}. These field strengths are about an order of magnitude weaker than the fields around ionic colloids[33,34], membranes[35], reverse micelles[36], or polyelectrolytes[37], but are comparable to experimental fields in ionic channels[38] or near AFM tip and can be safely manipulated in thin-layer AC and DC capacitance measurements.[39] Noteworthy, they also fall below the strengths that warrant the use of field-dependent polarizability correction in applications of the BK3 model of water.[40]

Technical details

We apply periodic boundary conditions in lateral directions to mimic a nanopore of infinite (x,y) dimensions, and we calculate electrostatic interactions by the slab-corrected Ewald method of Yeh and Berkowitz[41], where an empty space of 10 nm is inserted between the images along z direction. We use the real-space cutoff value R_c = 9.8 Å and the screening parameter $\alpha = \pi/R_c$, along with 15 × 15 × 45 vectors in the reciprocal space (k_x, k_y, k_z). The tail corrections to the Lennard-Jones and EXP6 interactions are treated by the method from our earlier work.[4] The insertion/deletion grand canonical step was divided into 5 intermediate processes for water and 20 steps were used for ion pairs in the preliminary electrolyte simulations. Parameter R_s from Eq. (1) was 0.25 nm. The positions of Drude particles of the BK3 FF in each configuration were found using a simple iteration terminated after none of the Drude particles moved more than 0.001 Å per iteration, typically this required 4-5 iterations with a negligible numerical error in the potential energy.

Monte Carlo. We simulate confined water using the Expanded Ensemble Grand Canonical Monte Carlo (EEGCMC) method. The method, relying on fractional particle exchanges, along with iterative determination of suitable biasing potential[42], has been used in several previous studies of pure water and electrolyte solutions confined in planar pores comprised of neutral hydrophobic walls[4,43] at different thermodynamic conditions including external electric fields.[5] A detailed description of the method is found in Ref.[4]; here we provide only a brief explanation and technical details relevant to its application to the BK3 model of water.[20]

The EEGCMC method simulates a solution (or pure substance) at specified confinement volume (corresponding to the width of the pore, h), temperature, T, and chemical potential values of all species constituting the solution, μ_i. As a result, equilibrium configurations from the corresponding grand canonical ensemble are obtained, and these are further statistically analyzed using standard methods to compute thermodynamic and structural properties, e.g., mean number densities, concentration, number density profiles, pressure tensor components and interfacial free energies. Considering an equilibrium between the confined solution and a solution in the bulk reservoir at specified values of T, molality, m_{bulk}, and pressure, P_{bulk}, the input chemical potentials μ_i must be equal to those in the bulk reservoir. These input chemical potentials are calculated in a separate bulk simulation prior to the simulation in confinement. Due to very

inefficient conventional grand canonical moves in aqueous solutions, particle insertions/deletions are realized in a sequence of subprocessess corresponding to virtual intermediate reactions between fractional particles that are only partially coupled to the system[4,6,44,45]. Here, we study aqueous confinements using the polarizable BK3 force field (FF) for water and NaCl ions[19,20], whose simulations are technically difficult and computationally expensive:

First, due to the polarizability the potential energy calculation of a system of polarizable particles cannot be separated to pair wise contributions. This renders conventional one-particle MC moves inefficient. We thus use Multiple-Particle (MPM) MC moves[14,17,46] for translations and rotations of all simulated particles simultaneously. This method has been shown to perform an order of magnitude faster when compared with the conventional one-particle MC moves, and it is also easily parallelizable. Alternatively, one can use molecular dynamics (MD), which, however, is technically more difficult when used in combination with the expanded grand canonical ensemble, and was thus not used here. We have, however, used MD calculations in a set of confined NaCl systems with fixed composition.

Second, the polarizable model introduces additional energetic contributions, which must be treated correctly in the expanded ensemble. Conveniently, the scaling scheme introduced in our previous work[4,44] can be used without any changes. The original scheme scales a general interaction potential $u(r_{ij})$ between two particles (two interaction sites) i and j with coupling parameters λ_i and λ_j, separated by the distance r_{ij}, as follows:

$$u(r_{ij},\lambda_i,\lambda_j) = \lambda_i\lambda_j u([r_{ij}^2 + R_s^2(1-\lambda_i\lambda_j)^2]^{1/2}) \quad (2)$$

where R_s is a constant parameter comparable to molecular size and the λ values are from the interval (0, 1) corresponding to (uncoupled ideal gas particle, fully coupled particle). We note that this scheme applies solely to the intermolecular interactions and has no impact on intramolecular contributions (*e.g.* the potential energy of Drude springs).[6] We also note that long range electrostatics[19,22] is not affected by the second term in the argument of u in Eq. (1), which means that long ranged Ewald summation contributions are only scaled by the product of pertinent λ values, equivalent to simply scaling magnitudes of the interacting charges.[6]

Our confined systems maintain equilibrium with (implicit) bulk reservoir at T = 298.15 K and P_{bulk} = 1 bar. The corresponding chemical potentials are adopted from our previous work.[6] In

neat water, μ_{H2O} = -237.2 kJ/mol, which contains the ideal gas contribution taken from the NIST-JANAF thermochemical tables, μ_{H2O}^{o} = -228.582 kJ/mol. [47]

Molecular Dynamics. In a set of selected situations, we studied solution structures using NVT Molecular Dynamics (MD) simulations. We used GROMACS 2018.4 to simulate SPC/E water with Joung Cheatham (JC) ions.[21,22] Due to a software incompatibility, simulations using the polarizable BK3 water model with AH ions, or BK3-AH[19,20], in confinement was performed using MACSIMUS, which is written and maintained by Jiri Kolafa.[48]

These simulations were performed using pore compositions corresponding to unperturbed bulk electrolyte concentration of 2.0 mol kg^{-1} obtained from EEGCMC results and were used to gain a better understanding of the structure within the pore over a longer period of time. The system was subjected to external electric fields of various strengths which are described in the models section. All MD simulations were 10 ns in length and performed using smooth walls, described in the next section, with 1.64 nm separation. Periodic boundary conditions were used with cutoffs of 9.8 Å and 10.0 Å for fixed-charge and polarizable models, respectively. Long ranged electrostatic interactions for the fixed-charge model were calculated using fast smooth Particle-Mesh Ewald summation[49] and the polarizable model utilizes the classical Ewald summation. Both models employ the appropriate correction[41] to account for the 2-D periodicity in the slab geometry. The timestep in the MD simulation was 2 fs. Nose-Hoover thermostat was used to keep the temperature at 298 K.

III. RESULTS AND DISCUSSION

A. Thermodynamics

Thermodynamic properties and water absorption presented as functions of the average electric field, $\langle E_f \rangle$, spanning the width of the water film d_f (the width of the region with nonzero average charge density from the H_2O atoms), are shown in Figure 2. The *averaged* electric fields $\langle E_f \rangle$ correspond to imposed electric displacement fields D_z listed along with the corresponding $\langle E_f \rangle$ values in Table I. Somewhat stronger $\langle E_f \rangle$ values are shown in the case of molecular walls where d_f includes a low-water-density region associated with slight penetration of water between the hydrophobic chains of the walls. In the SW system, the *field dependence* of water uptake inside the pores is weaker for BK3 than for SPC/E water but the total absorption is higher for

BK3 water. When molecular walls are used, the dependence on the electric field appears to be similar for both water models; however, larger error bars associated with compute-intense BK3 runs prevent a definitive statement for this model. As shown in detail in forthcoming Figures (3-9), the structure of confined water shows subtle differences between the two models with the polarizable model providing a more realistic picture in the presence or absence of an electric field.

A larger pressure normal to the walls is observed for SPC/E water with a tendency to increase with increasing field strength for both models. The trend of increasing pressure, associated with increased uptake of water in the pore upon increasing field strength holds true for both wall types. Significant difference between wetting free energies are present between the two wall types. In addition, SPC/E has a lower wetting free energy using molecular walls but smaller differences are present between the two water models for SW. Results for the polarizable

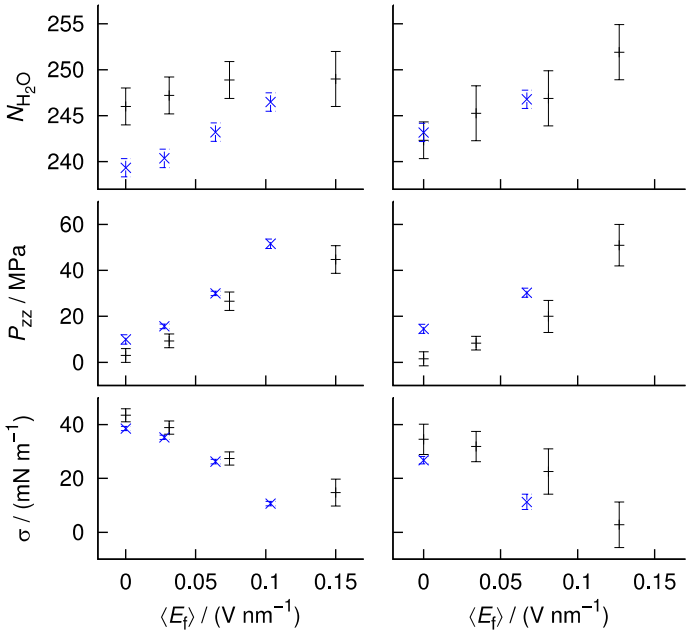

Figure 2. The dependence of the average numbers of water molecules (top), normal pressure (middle) and interfacial tension σ (bottom) on the strength of the average electric field across the aqueous slab in BK3 (black) or SPC/E (blue symbols) molecules between smooth (left) or butyl-coated walls (right) in GCMC simulations maintaining equilibrium between the pore and a bulk reservoir of water at ambient conditions.

model, however, are still consistent with the wetting behavior noted in our previous papers based on the nonpolarizable representation.[4,5,26]

B. Structure

While the properties of unperturbed bulk water may be properly described regardless of whether the molecular polarization is taken into account, the effects of molecular polarizability on structural properties become more important once water is placed in a confinement and especially when subjected to an external electric field. In the left column of Figure 2, we compare the difference in water uptake into a SW system with wall separation of 1.64 nm between SPC/E and BK3 water models. There is a noticeable increase in the number of water molecules absorbed into the pore when using the polarizable model, Fig. 2, which in turn leads to a more pronounced structure at the interface, Fig. 3. In both cases the ordering of water molecules persists throughout the pore as one would expect from previous works.[4,5,26] The enhanced peaks near the interface for BK3 water is likely a crowding effect due to the increase in the overall density within the pore. In addition, there is a marked difference between the two models once an external field is applied. SPC/E water shows a much stronger polarity dependence on the field, which is evidenced by the strongly depleted peak near the right wall, where the field is pointing toward the wall. The presence of Gaussian charges on springs reduces the polarity dependence because the more flexible charge distribution is well suited to accommodate both the orientational water-wall preferences and the dipole alignment with the field.

The inherent weakness of fixed charge models is the inability of their charge distribution to respond to physical changes in a system. Our results shown in Fig. 4 reveal a notable difference in the average molecular dipole moments between the bulk phase water and water near the interface both with or without the presence of an electric field (Fig. 4). While average dipole moments of both SPC/E, 2.35 D, and BK3, 2.64 D, water are lower than the experimental value, 3.0 D, a reduction in the average dipole moment of over 10% near the interface can be seen, which is consistent with previous first principles studies.[20,50-53] In the case of the molecular walls, water is able to somewhat penetrate into the gaps between butyl-chains overcoming the weak steric hindrance.

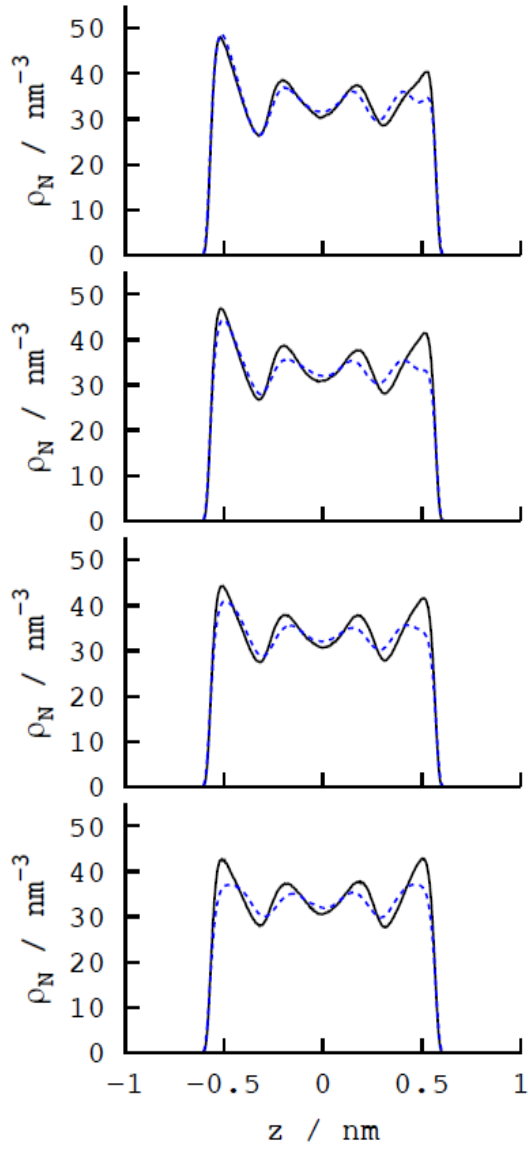

Figure 3. Density distributions of BK3 (black) or SPC/E (dashed blue) molecules across the nanopore between a pair of smooth walls at separation 1.64 nm in equilibrium with the bulk phase at ambient conditions in the absence (bottom), or presence of perpendicular fields (directed from the left to the right wall) of strengths (from bottom to top) D_z =0.0, 0.00885, 0.0177 and 0.0266 C m^{-2}. Statistical uncertainties are of the order of ±1%.

This effect, illustrated in Fig. 1, is enhanced in the presence of an electric field and can play a role in somewhat different reductions of the dipole moment of BK3 molecules at the SW and MW interfaces.

While water orientations are biased, as expected[23,24], next to confining walls, there is a *significant* difference in the extent of spontaneous orientation of interfacial molecules when using a nonpolarizable model and a polarizable model. In Figure 5 we display water's orientation in terms of cosine of the angle formed between the dipole of water and the direction of the electric field, which is normal to the plates. In both cases water orients similarly in the intermediate region between the plates; however, the region of interest is near the interface.

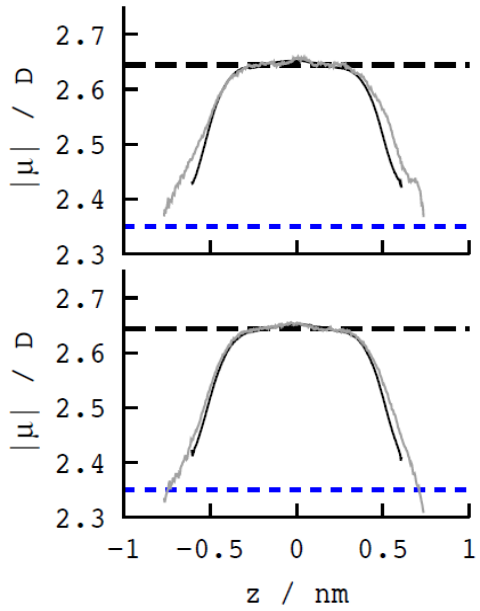

Figure 4. The average magnitude of the molecular dipoles of BK3 (solid curves) molecules as functions of the position inside the pore in the absence (black) or presence of electric displacement field of strength 0.0266 C m^{-2} (grey) between smooth (bottom) or molecular (butyl-coated) walls (top) in GCMC simulations maintaining equilibrium between the pore and a bulk reservoir of water at ambient conditions. Horizontal lines correspond to bulk values of the dipoles of BK3 (black long dashed) and SPC/E (blue short-dashed) molecules.

Under zero field it is evident that water orientation-bias near the interface is more dramatic for the fixed-charge model, than for the polarizable model. It is possible that for this reason, water exhibits the behavior seen in Figure 3, showing the tendency toward the right-hand-side (field pointing toward the wall) peak depletion is much more prominent in the fixed charge model. Lastly, the structure near the interface for the polarizable model persists for a slightly longer

distance as evidenced by the slight shift in first and last peak locations and the requirement of a stronger field to elicit a similar response in dipole orientation to that of the SPC/E water. Additionally, even at higher field strengths the orientation between the two models differ. Notable charge oscillations as a result of the difference in the atom densities associated with the orientations of water molecules are present for both models studied, in analogy with previous works.[4,5,23] We use two distinct metrics of charge distribution in BK3 water: in one, we ascribe

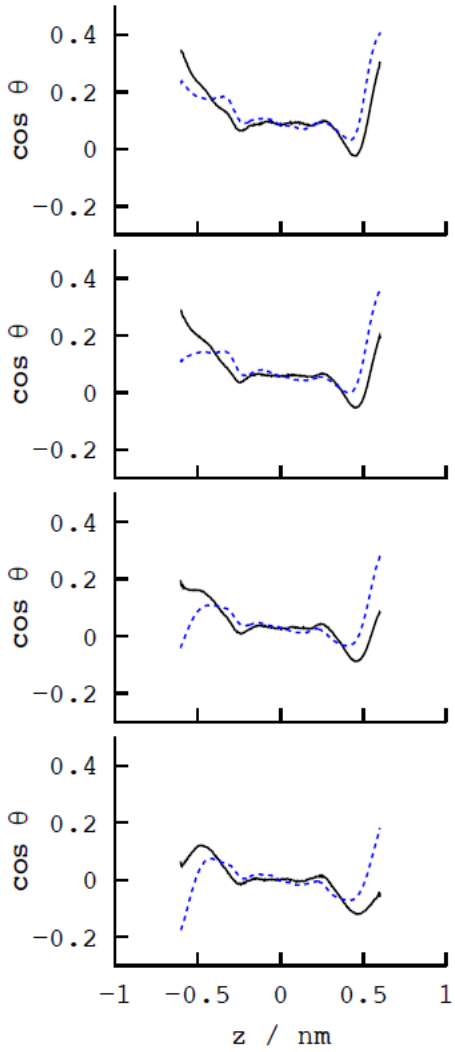

Figure 5. The average orientation of molecular dipoles of BK3 (black curves) or SPC/E molecules (dashed blue) measured in terms of the angle θ between the dipole and the direction of the field (normal to the walls) as functions of the position inside the pore at electric displacement fields D_z=0.0, 0.00885, 0.0177 and 0.0266 C m^{-2} (from bottom to top) between smooth walls in GCMC simulations maintaining equilibrium between the pore and a bulk reservoir of water at ambient conditions.

entire atomic charges to the charge site positions and in the other we explicitly account for the Gaussian distribution of the charges. When comparing the charge densities between the two models based on only point-charges in Figure 6, we can observe peaks near the walls to be similar in both height and location for no electric field. Peaks in the middle of the system are slightly shifted and with reduced peak amplitude for SPC/E water, which is a trend that persists when we apply an electric field. In addition, a greater difference between the peaks near the interfaces is observed, with increasing electric field strengths, for SPC/E water than for BK3 water. This reduced effect on BK3 water is especially noticeable when we explicitly account for the Gaussian distributions. Large shifts in the peak locations and amplitudes occur once the Gaussian distributions are accounted for, which results in a slightly more smoothed out distribution with smaller oscillations. These peak shifts effectively switch the profiles when relating charge distributions for BK3 water and SPC/E water. The rightmost peaks are enhanced under an electric field for the point-charge calculations, while the Gaussian density distribution shows enhancement of the leftmost peak, which corresponds more directly to the changes in the density profile shown in Figure 3. Furthermore, positive values for the Gaussian distribution are in similar positions as oxygen in Figure 3, which is not the case for point-charge densities.

Similar trends to the simulation using SW can be observed when utilizing molecular walls at separation of 2.81 nm, which results in a pore size of approximately 1.64 nm (Figure 7). However, water molecules can somewhat penetrate and reside between the butyl groups that coat the graphane surface. The residence time the molecules remain trapped inside the brush increases upon applying an electric field. For molecular walls, there is more room for water to orient near the butyl groups which results in a much smoother drop in the density profile. In addition, the enhancement of the left-most peak and subsequent depletion of the right-most peak corresponding to water near the left wall and right wall, respectively, more closely resembles the density profile of BK3 water on SW. That is, the depletion of the right peak is not as profound as observed with the SPC/E model. This is due to the maximal orientation bias when the wall is smooth and the molecules feature a rigid distribution of atom charges. A rough wall renders many orientations acceptable at parts of the surface. The overall results for molecular walls are consistent with our previous work.[4,5]

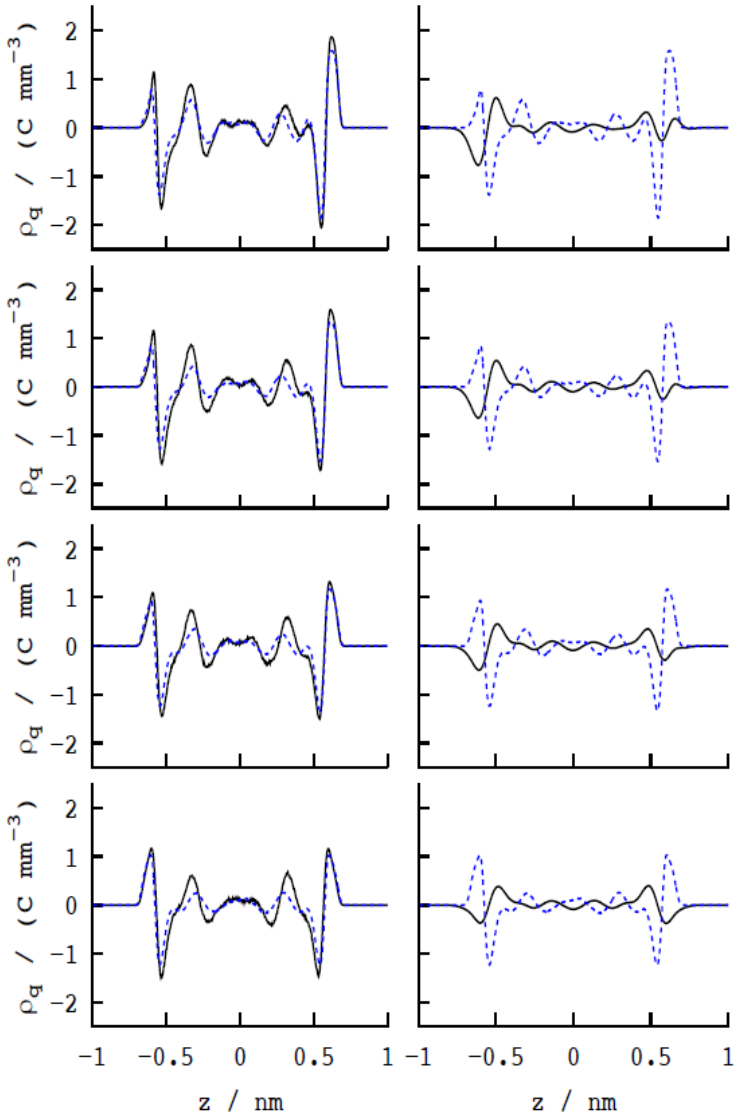

Figure 6. The average charge density profiles of BK3 (black curves) or SPC/E (dashed blue) molecules (dashed blue curves) as functions of the position inside the pore at fields D_z =0.0, 0.00885, 0.0177 and 0.0266 C m^{-2} (from bottom to top) between smooth walls in GCMC simulations maintaining equilibrium between the pore and a bulk reservoir of water at ambient conditions. Charge densities are calculated by placing entire charges at charge site centers (left) or by explicitly accounting for the Gaussian charge distributions in the BK3 model (right).

We now turn to the comparison between molecular orientations at the two wall types (SW and MW). The differences in average molecular orientations, both with and without electric field, observed near the interface may derive from the softer interaction with the butyl groups. However, the differences in average orientation with respect to the electric field are not as

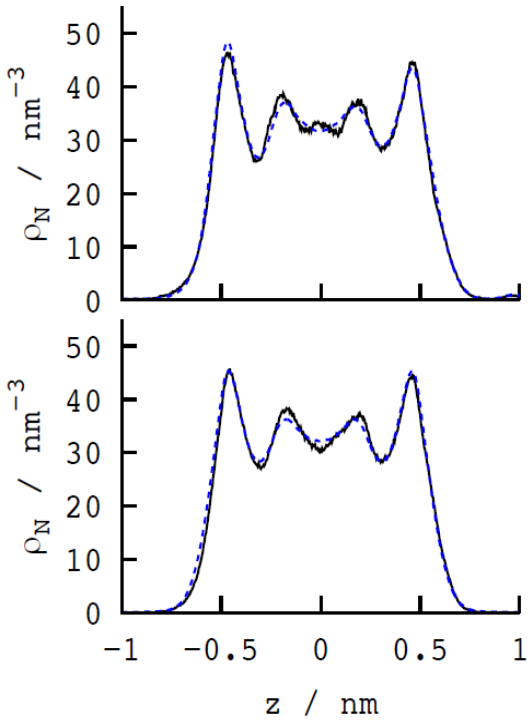

Figure 7. Density distributions of BK3 (black) or SPC/E (dashed blue) molecules across the nanopore between a pair of butyl-coated graphane walls at separation 2.81 nm in equilibrium with the bulk phase at ambient conditions in the absence (bottom), or presence of perpendicular field (directed from the left to the right wall) of strength D_z=0 (bottom) or 0.0266 C m^{-2} (top). Statistical uncertainties are of the order of ±1%.

profound as those found in the density profiles of Figure 3. This in combination with the overall difference in dipole orientations near the interface confirm that the ability to polarize in response to a field is crucial to get a sense of both dynamic and structural properties in confined water. Penetration into the alkyl brush can also be observed when looking at the average charge density profiles in Figure 9 as observed elsewhere.[5] In both SPC/E and BK3 models this penetration is

present; however, a more ordered structure becomes evident for BK3 water when an electric field is applied. This order extends even into the butyl groups and is present when Gaussian charges are explicitly considered. In this case, the asymmetry of the charge density distribution seems to be greater for the SPC/E model with an extra peak present near the right wall which is smoothed over for the Gaussian charge calculation. Shifts in peak positions and amplitudes persist as was the case in the SW implementation; however, the profiles are not swapped. Meaning, the enhanced peaks remain near the same wall for both charge density calculation methods. Because of more effective balancing of positive and negative contributions from smeared gaussian charges, the nonzero charge density between the butylated walls spans a wider region with the SPC/E model notwithstanding similar oxygen atom distributions.

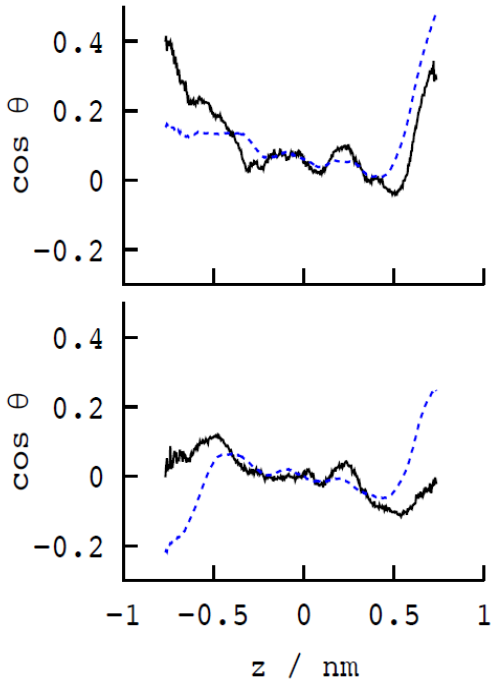

Figure 8. The average orientation of molecular dipoles of BK3 (black curves) or SPC/E molecules (dashed blue) measured in terms of the angle θ between the dipole and the direction of the field (normal to the walls) as functions of the position inside the pore at fields $D_z = 0.0$ C m^{-2} (bottom) and $D_z = 0.0266$ C m^{-2} (top) between butyl-coated walls in GCMC simulations maintaining equilibrium between the pore and a bulk reservoir of water at ambient conditions.

Charge density contributions for H and O atoms have been individually calculated in Figure 10 for comparison to the average local charge densities. For BK3 water, calculations were

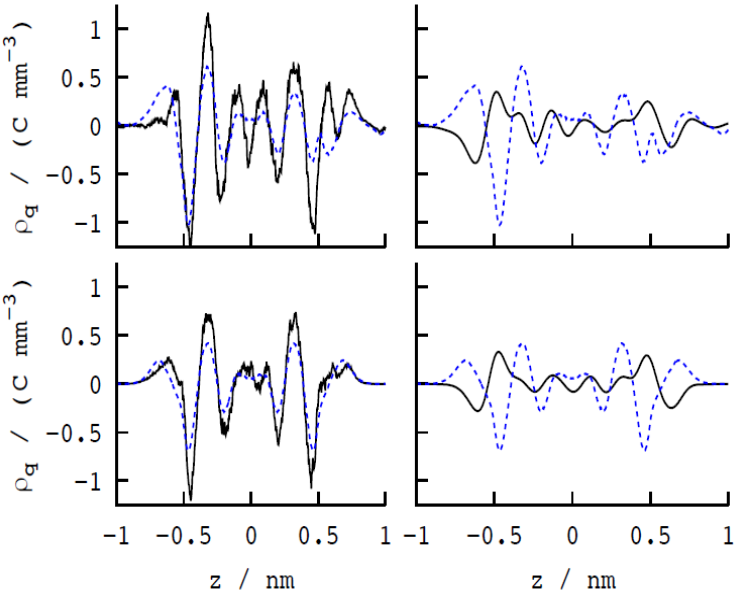

Figure 9. The average charge density profiles of BK3 (black curves) or SPC/E (dashed blue) molecules (dashed blue curves) as functions of the position inside the pore at fields D_z=0 (bottom) or 0.0266 C m^{-2} (top) between butyl-coated walls in GCMC simulations maintaining equilibrium between the pore and a bulk reservoir of water at ambient conditions. Charge densities are calculated by placing entire charges at charge site positions (left) or by explicitly accounting for the Gaussian charge distributions in the BK3 model (right).

performed both by placing point-charges on molecular sites and by explicitly accounting for Gaussian distributions of charge. Only point-charge calculations can be performed for SPC/E water. Comparison between point-charge calculation yield little difference between the models, with only slightly sharper peaks for BK3 water. This peak pronunciation is greatly lessened, however, when observing the slit charge density profiles due to the Gaussian charges, which results in overall smaller density amplitudes and peak shifts compared to SPC/E water. The origin of the essentially flipped charge density profile, discussed in Figure 6, for Gaussian charges becomes a bit clearer with the smoothing of the larger negative charge build up for the point-charge model near the wall.

It is of interest to note the polarizability-induced changes in *atom* density profiles (Figs. 3 and 7) are much milder than the changes in the corresponding charge-density distributions. The main reason for the relative insensitivity of the actual liquid structure is the fact that steric forces

keep charged atoms at separations well above the width of the Gaussian charges, thus the difference between the interactions among point charges and those of the Gaussian form is much smaller than could be inferred from the charge-density profiles along a single coordinate while averaged over the remaining (lateral) directions.

The knowledge about the charge density profiles such as those illustrated in Fig. 9 can be used in the characterization of the dielectric response of the confined polar liquid. For this purpose, we monitor the effective width of the water slab between the walls, d_f, defined as the width with nonvanishing density of charges from hydrogen and oxygen atoms. The values of d_f observed in our simulated systems are collected in Table I. Using the test-charge method, <ref. 5>, we also sampled the average voltage drop $\langle U \rangle$ between the opposite wall positions separated by the distance h. In our model system, any dielectric screening occurs within the slab layer of

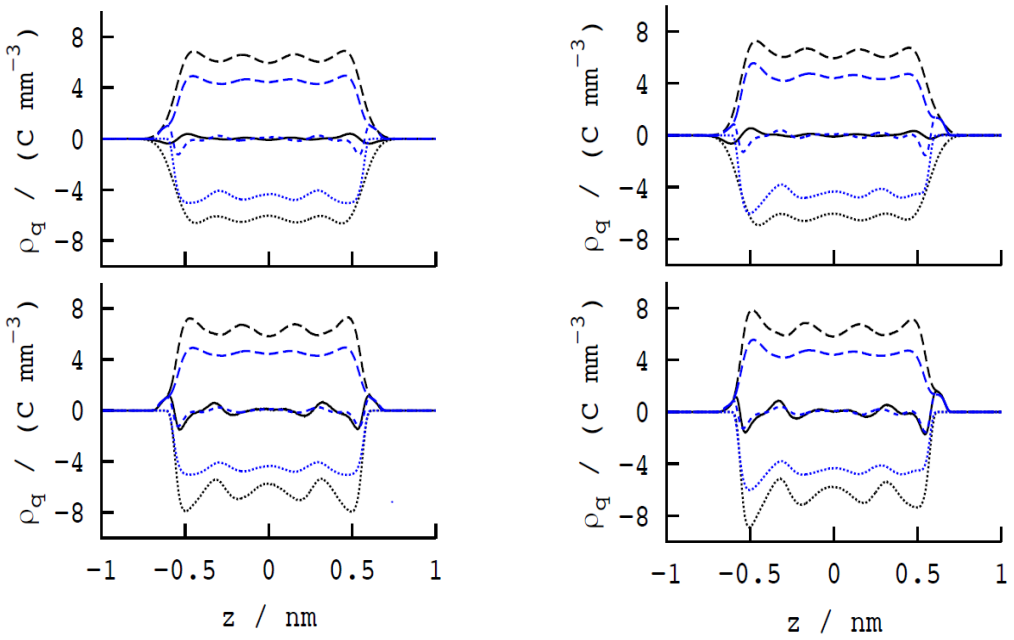

Figure 10. The H (long-dashed) and O (dotted) contributions to local charge density $\rho_q(z)$ for BK3 (black) and SPC/E (blue) water models, and total charge-density profiles of BK3 (solid black curves) or SPC/E molecules (short dashed blue curves) as functions of the position inside the pore between smooth walls in GCMC simulations maintaining equilibrium between the pore and a bulk reservoir of water at ambient conditions. The left graphs are obtained in the absence and the right ones in the presence of electric field of strength D_z=0.0266 C m^{-2}. Individual contributions from oxygen and hydrogen atoms greatly exceed the total densities. Charge densities are calculated by placing entire charges at charge site positions (bottom) or by explicitly accounting for the correct Gaussian charge distributions in the BK3 model (top). The former method shows small differences between the two models, whereas the actual densities due to the Gaussian charges in the BK3 model feature smoother profiles with reduced amplitudes and a considerable shift of the extrema relative to the distributions of point-charges.

width d_f. The difference between the actual voltage $<U>$ and the expected voltage in vacuum, $U_o=D_z h/\varepsilon_o$ alows us to estimate the effective dielectric constant along the direction normal to the walls, $\varepsilon_f \equiv <\frac{1}{\varepsilon_\perp(z)}>_{d_f}^{-1} = (1 - \frac{<U>-U_o}{U_0}\frac{h}{d_f})^{-1}$, as well as the average field $E_f = U_0 / h\varepsilon_f$, both averaged over the thickness of the aqueous slab d_f. Table I collects the simulated voltages, effective dielectric constants, and average electric fields E_f exerted on water molecules in the confinement. Despite statistical uncertainties of the above estimates, our data consistently show a reduction in the permittivity of *confined* polarizable water below that of the nonpolarizable model. The opposite holds true for dielectric constants of the two models in the bulk phase, where $\varepsilon_{BK3} > \varepsilon_{SPC/E}$. The reversal is explained by two effects: a) the reduction of the dipole moment of interfacial BK3 molecules relative to the bulk value (See Fig. 4), causing a decrease of ε_f in narrow confinements where a significant fraction of the molecules is affected, and b) the blurred amplitudes of the BK3 charge density profiles (Figs. 6 and 9) along the wall normal z, $\rho_q(z)$, due to the considerable overlapping of gaussian charges *projected* on z axis. The true (3-D) overlap between these charges is, of course, minimal due to steric exclusion, as charges with centers at similar positions z remain well separated in the lateral (x, y) directions.

Comparisons between the results for ε_f between smooth and molecular walls also indicate an additional reduction of the dielectric constant when water is confined between molecular (alkyl-coated) walls (MW). This reduction, consistently observed with both polarizable and nonpolarizable models of water, reflects the ability of water molecules to sporadically penetrate between the molecular chains on the walls. Rare penetration events increase the apparent film thickness d_f resulting in lower average ε_f while the dielectric properties inside the rest of the film remain unaffected.

The Expanded Ensemble Grand Canonical Monte Carlo (EEGCMC) simulations of electrolyte solutions have proven too costly for systematic studies of bulk-confinement equilibria of salt solutions using the polarizable force field. To assess the importance of molecular polarizabilities on the structure of confined electrolytes, we performed Molecular dynamics simulations in closed (NVT) systems with selected compositions suggested from previous EEGCMC simulations. In BK3-AH simulations described in Figure 11, we use initial configurations obtained from MD runs employing the SPC/E-JC model with a bulk equilibrium

Table I. EE-GCMC results for the actual voltage $<U>$ across open pores of width h (1.64 nm for smooth walls and 2.82 nm for alkyl-coated walls) equilibrated with a field-free bulk phase. The pores are spanned by electric displacements fields D_z, corresponding to the vacuum (unscreened) voltages U_o, and $<U>$ is the actual voltage. $<U>$ reflects the screening inside the film with nonzero charge density arising from partial charges on water molecules. The width of the film d_f is between 1.45 and 1.66 Å. $<U_f>$ is the potential difference across the film, $<E_f>$ the mean electric field, and $\varepsilon_f = <\frac{1}{\varepsilon_\perp(z)}>_{d_f}^{-1}$ the effective dielectric constant along the pore normal, averaged over the film width d_f. Black: smooth walls, blue: alkyl-coated walls, bold: polarizable (BK3) force field.

System:	$\frac{m_{bulk}}{\text{mol kg}^{-1}}$	$\frac{D_z}{\text{Cm}^{-2}}$	$\frac{h}{\text{nm}}$	$\frac{d_f}{\text{nm}}$	$\frac{U_o}{\text{V}}$	$\frac{<U>}{\text{V}}$	$\frac{<U_f>}{\text{V}}$	$\frac{<E_f>}{\text{V nm}^{-1}}$	ε_f
SPC/E	-	0.00885	1.64	1.45	1.64	0.230	0.040	0.028	36
SPC/E	-	0.0177	1.64	1.45	3.28	0.473	0.093	0.064	31
SPC/E	-	0.0266	1.64	1.45	4.92	0.720	0.150	0.103	29
SPC/E-JC	1.0	0.0177	1.64	1.45	3.28	0.464	0.084	0.058	35
SPC/E-JC	2.0	0.0177	1.64	1.45	3.28	0.455	0.075	0.052	39
BK3	-	0.00885	1.64	1.45	1.64	0.236	0.046	0.032	**32**
BK3	-	0.0177	1.64	1.45	3.28	0.487	0.107	0.074	**27**
BK3	-	0.0266	1.64	1.45	4.92	0.790	0.22	0.152	**20**
SPC/E	-	0.0177	2.82	1.65	5.64	2.45	0.117	0.071	28
SPC/E-JC	1.0	0.0177	2.82	1.65	5.64	2.43	0.097	0.059	34
SPC/E-JC	4.0	0.0177	2.82	1.65	5.64	2.44	0.110	0.076	31
BK3	-	0.00885	2.82	1.57	2.82	1.30	0.054	0.034	**29**
BK3	-	0.0177	2.82	1.59	5.64	2.58	0.128	0.081	**25**
BK3	-	0.0266	2.82	1.66	8.45	3.68	0.211	0.127	**24**

reservoir concentration of ~2 mol kg^{-1} and a pore with smooth walls under no electric field. Charge density distributions are calculated using both the point-charges and using explicitly calculated Gaussian distributions. Ions tend to reside in the center of the pore as was found in previous works.[5,54] Ions are slightly more structured for the BK3-AH model with little change in

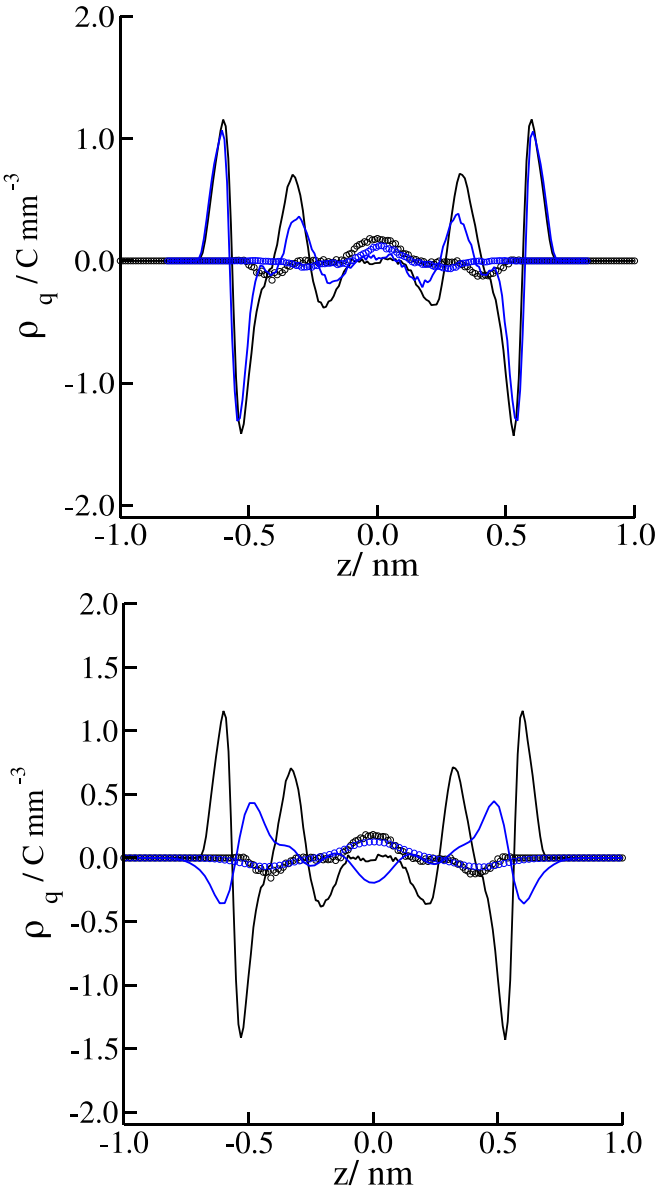

Figure 11. Top: The average charge density profiles due to BK3 (black lines) or SPC/E (blue lines) water molecules and polarizable NaCl ions in BK3 water (black circles) or JC ions in SPC/E (blue circles) solvent in a field-free nanopore with smooth walls and equilibrium reservoir concentration of ~2 mol kg^{-1}. Bottom: comparison between the profiles for BK3-AH solutions from the top graph (black lines and symbols) and the results obtained in the same system when explicitly accounting for the Gaussian charge distributions of the BK3-AH system. Overlapping Gaussian distributions reduce the density amplitudes of

water and visibly shift the extrema of water contribution. A slight smoothing of the salt charge distribution is present.

charge distribution when Gaussian charges are taken into account. Charge distribution for water remains virtually the same for both models near the surface, but the same small shift, as in Figure 6, in density can be observed for the inner peaks. A reduction of density amplitudes and shifts, similar to those noted with Figures 6 and 9, can be observed when accounting for the Gaussian distributions of atom charges.

The system described in Figure 12 was subjected to a field, D_z, of 0.0177 C m^{-2}. The asymmetric response to the electric field is analogous to that in pure water[5]. Despite a noticeable

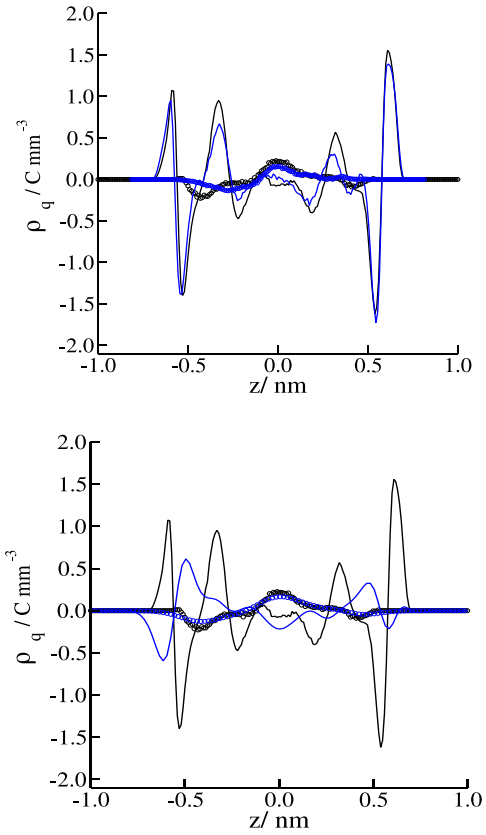

Figure 12. Top: The average charge density profiles due to BK3 (black lines) or SPC/E (blue lines) water molecules and polarizable NaCl ions in BK3 water (black circles) or JC ions in SPC/E (blue circles) solvent nanopore with smooth walls under electric displacement field, D_z =0.0177 C m$^{-2,}$ corresponding to a field-free reservoir with NaCl concentration of ~2 mol kg^{-1}. Bottom: comparison between the profiles for BK3-AH solutions from the top graph (black lines and symbols) and the results obtained in the BK3-AH system (blue) when explicitly accounting for the Gaussian charge distributions of mobile charges (blue).

redistribution of the ions, their tendency to reside in the center of the pore is unchanged. Notably, the ion response to the field is more pronounced in the polarizable model, suggesting this representation can be superior in studies of electric double layer, especially at the quantitative level. Overall, the structured AH ion profile is similar as in the absence of the field, but the smoothing of the charge distribution resulting from explicitly calculating Gaussian charge densities is more evident. Water peak enhancement due to the field follows a similar trend as in Figures 6 and 9, showing flipped enhancements between the charge density profiles resulting from the point-charge model and the Gaussian charge model, with the latter being relevant for the overall dielectric response in confined polarizable liquid.

IV. CONCLUDING REMARKS

Neglect of molecular polarizability can be a serious simplification in modeling aqueous interfaces under the influence of electric fields from ions or an external source. To assess the importance of the effect, we performed molecular simulations of a nanoporous model system permeated by water or salt solution modeled by two distinct force fields. We used the nonpolarizable extended simple charge model (SPC/E) along with Joung-Cheatham model for ions, and the polarizable BK3-AH model, which treats partial charges as Gaussian charge clouds attached to atoms by harmonic springs. Our model liquid was placed between a pair of hydrocarbon-like plates with weak wetting propensity to monitor the field-induced changes of water uptake from the bulk environment. We also monitored the variation of confinement pressure and interfacial tension, as well as atom and charge density distributions in the pores.

Regardless of the external field, we find the mean dipoles of interfacial water molecules are about 10% lower than in the bulk phase when using the polarizable model. The observed reduction is in good agreement with the prediction from the first principles calculations for water/vapor interfaces. The smeared atomic acharges of the polarizable model, intended to mimic the electronic distribution in real molecules, result in shifted extrema and lowered amplitudes of charge density profiles across the nanopores, weakening the liquid dielectric

response. In pure water, the above confinement effects result in reduction of the permittivity of polarizable-model water relative to the nonpolarizable one. Although the permittivity of the polarizable BK3 model in the bulk phase is over 10% higher than that of the nonpolarizable

(SPC/E) one, the order is reversed in the confinement where the average permittivity of the polarizable water falls around 20% below the value for the nonpolarizable model. Conversely, in the presence of dissolved salt, molecular and ion polarizabilities enhance the electric double layer response to the field.

The pronounced changes in the charge density distributions, averraged over the cross-section of the pores, are not accompanied by comparable changes in the intermolecular potentials since interatomic steric exclusion prevents any significant overlap between the gaussian charges on adjacent atoms. As a result, we observe only moderate changes of selected thermodynamic properties and the liquid density profiles across the pore. Open ensemble simulations of the pore-bulk phase equilibrium reveal a stronger pore absorption of polarizable water in the absence of the applied electric field, whereas the field-induced enhancement of water uptake is bigger in the nonpolarizable model. The strong effects of field direction, previously revealed in a nonpolarizable system, are weaker with the polarizable model, which is better suited to reconcile the competing trends of spontaneous and field-induced orientations in interfacial water. The above differences warrant the consideration of polarizable force fields for studies of confined water and solutions. Methodological improvements will be required to extend the present open ensemble (Expanded Ensemble Grand Canonical) simulations of pore-environment equilibria in neat water to systematically study open electrolyte systems in polarizable representation.

ACKNOWLEDGEMENTS

We thank Jiri Kolafa for his help with the MACSIMUS package. While performing this work, SZ, DB and AL were supported by the Office of Basic Energy Sciences, Chemical Sciences, Geosciences, and Biosciences Division of the U.S. Department of Energy (Grant No. DE-SC 0004406) and FM was supported by Czech Science Foundation (Grant No. 19-05696S). A.L. also acknowledges support from the National Science Foundation under Grant No. CHE-1800120 in the final phase of the study. We thank for the supercomputer time from Extreme Science and Engineering Discovery Environment (XSEDE), supported by NSF Grant No. OCI-1053575, and the National Energy Research Scientific Computing Center (NERSC), supported by the Office of Science of the U.S. Department of Energy (DEAC02-05CH11231). Access to computing and storage facilities owned by parties and projects contributing to the National Grid Infrastructure MetaCentrum (programme "Projects of Large Research, Development, and Innovations Infrastructures, CESNET LM2015042), is greatly appreciated.

REFERENCES

[1]C. Vega and J. L. F. Abascal, Simulating water with rigid non-polarizable models: A general perspective, *Phys. Chem. Chem. Phys.* **13**, 19663 (2011).

[2]W. R. Smith, I. Nezbeda, J. Kolafa, and F. Moucka, Recent progress in the molecular simulation of thermodynamic properties of aqueous electrolyte solutions, *Fluid Phase Equilib.* **466**, 19 (2018).

[3]J. C. Rasaiah, S. Garde, and G. Hummer, Water in nonpolar confinement: From nanotubes to proteins and beyond, *Annu. Rev. Phys. Chem.* **59**, 713 (2008).

[4]F. Moucka, D. Bratko, and A. Luzar, Electrolyte pore/solution partitioning by expanded grand canonical ensemble monte carlo simulation, *J. Chem. Phys.* **142**, 124705 (2015).

[5]F. Moucka, D. Bratko, and A. Luzar, Salt and water uptake in nanoconfinement under applied electric field: An open ensemble monte carlo study, *J. Phys. Chem. C* **119**, 20416 (2015).

[6]F. Moucka, I. Nezbeda, and W. R. Smith, Chemical potentials, activity coefficients, and solubility in aqueous nacl solutions: Prediction by polarizable force fields, *J. Chem. Theory Comput.* **11**, 1756 (2015).

[7]K. Kiyohara, K. E. Gubbins, and A. Z. Panagiotopoulos, Phase coexistence properties of polarizable water models, *Mol. Phys.* **94**, 803 (1998).

[8]M. Predota, A. A. Chialvo, and P. T. Cummings, On the determination of the vapor-liquid envelope for polarizable models by monte carlo simulation, *Fluid Phase Equilib.* **183**, 295 (2001).

[9]M. Medeiros and M. E. Costas, Gibbs ensemble monte carlo simulation of the properties of water with a fluctuating charges model, *J. Chem. Phys.* **107**, 2012 (1997).

[10]E. M. Yezdimer and P. T. Cummings, Calculation of the vapour-liquid coexistence curve for a fluctuating point charge water model, *Mol. Phys.* **97**, 993 (1999).

[11]S. W. Rick, S. J. Stuart, and B. J. Berne, Dynamical fluctuating charge force-fields - application to liquid water, *J. Chem. Phys.* **101**, 6141 (1994).

[12]B. Chen, J. H. Xing, and J. I. Siepmann, Development of polarizable water force fields for phase equilibrium calculations, *J. Phys. Chem. B* **104**, 2391 (2000).

[13]B. Chen, J. J. Potoff, and J. I. Siepmann, Adiabatic nuclear and electronic sampling monte carlo simulations in the gibbs ensemble: Application to polarizable force fields for water, *J. Phys. Chem. B* **104**, 2378 (2000).

[14]F. Moucka, M. Rouha, and I. Nezbeda, Efficient multiparticle sampling in monte carlo simulations on fluids: Application to polarizable models, *J. Chem. Phys.* **126**, 224106 (2007).

[15]F. Moucka and I. Nezbeda, Multi-particle sampling in monte carlo simulations on fluids: Efficiency and extended implementations, *Mol. Simul.* **35**, 660 (2009).

[16]F. Moucka and I. Nezbeda, Gibbs ensemble simulation on polarizable models: Vapor-liquid equilibrium in baranyai-kiss models of water, *Fluid Phase Equilib.* **360**, 472 (2013).

[17]F. Moucka, I. Nezbeda, and W. R. Smith, Computationally efficient monte carlo simulations for polarisable models: Multi-particle move method for water and aqueous electrolytes, *Molecular Simulation* **39**, 1125 (2013).

[18]W. L. Jorgensen and J. D. Madura, Temperature and size dependence for monte-carlo simulations of tip4p water, *Mol. Phys.* **56**, 1381 (1985).

[19]P. T. Kiss and A. Baranyai, A new polarizable force field for alkali and halide ions, *J. Chem. Phys.* **141**, 114501 (2014).
[20]P. T. Kiss and A. Baranyai, A systematic development of a polarizable potential of water, *J. Chem. Phys.* **138**, 204507 (2013).
[21]H. J. C. Berendsen, J. R. Grigera, and T. P. Straatsma, The missing term in effective pair potentials, *J. Phys. Chem.* **91**, 6269 (1987).
[22]I. S. Joung and T. E. Cheatham, Determination of alkali and halide monovalent ion parameters for use in explicitly solvated biomolecular simulations, *J. Phys. Chem. B* **112**, 9020 (2008).
[23]C. Y. Lee, J. A. McCammon, and P. J. Rossky, The structure of liquid water at an extended hydrophobic surface, *J. Chem. Phys.* **80**, 4448 (1984).
[24]J. C. Shelley and G. N. Patey, Boundary condition effects in simulations of water confined between planar walls, *Mol. Phys.* **88**, 385 (1996).
[25]D. Bratko, R. A. Curtis, H. W. Blanch, and J. M. Prausnitz, Interaction between hydrophobic surfaces with metastable intervening liquid, *J. Chem. Phys.* **115**, 3873 (2001).
[26]D. Bratko, C. D. Daub, K. Leung, and A. Luzar, Effect of field direction on electrowetting in a nanopore, *J. Am. Chem. Soc.* **129**, 2504 (2007).
[27]D. Bratko, C. D. Daub, and A. Luzar, Field-exposed water in a nanopore: Liquid or vapour?, *Phys. Chem. Chem. Phys.* **10**, 6807 (2008).
[28]D. Vanzo, D. Bratko, and A. Luzar, Wettability of pristine and alkyl-functionalized graphane, *J. Chem. Phys.* **137**, 034707 (2012).
[29]J. O. Sofo, A. S. Chaudhari, and G. D. Barber, Graphane: A two-dimensional hydrocarbon, *Physical Review B* **75**, 153401 (2007).
[30]D. C. Elias, R. R. Nair, T. M. G. Mohiuddin, S. V. Morozov, P. Blake, M. P. Halsall, A. C. Ferrari, D. W. Boukhvalov, M. I. Katsnelson, A. K. Geim, and K. S. Novoselov, Control of graphene's properties by reversible hydrogenation: Evidence for graphane, *Science* **323**, 610 (2009).
[31]C. D. Bain, E. B. Troughton, Y. T. Tao, J. Evall, G. M. Whitesides, and R. G. Nuzzo, Formation of monolayer films by the spontaneous assembly of organic thiols from solution onto gold, *J. Am. Chem. Soc.* **111**, 321 (1989).
[32]W. L. Jorgensen, J. D. Madura, and C. J. Swenson, Optimized intermolecular potential functions for liquid hydrocarbons, *J. Am. Chem. Soc.* **106**, 6638 (1984).
[33]J. Z. Wu, D. Bratko, H. W. Blanch, and J. M. Prausnitz, Effect of three-body forces on the phase behavior of charged colloids, *J. Chem. Phys.* **113**, 3360 (2000).
[34]J. Z. Wu, D. Bratko, and J. M. Prausnitz, Interaction between like-charged colloidal spheres in electrolyte solutions, *Proc. Natl. Acad. Sci.* **95**, 15169 (1998).
[35]D. Bratko, B. Jonsson, and H. Wennerstrom, Electrical double-layer interactions with image charges, *Chem. Phys. Lett.* **128**, 449 (1986).
[36]D. Bratko, C. E. Woodward, and A. Luzar, Charge fluctuation in reverse micelles, *J. Chem. Phys.* **95**, 5318 (1991).
[37]D. Bratko and D. Dolar, Ellipsoidal model of poly-electrolyte solutions, *J. Chem. Phys.* **80**, 5782 (1984).
[38]J. Dzubiella, R. J. Allen, and J. P. Hansen, Electric field-controlled water permeation coupled to ion transport through a nanopore, *J. Chem. Phys.* **120**, 5001 (2004).

[39]C. R. Song and P. S. Wang, High electric field effects on gigahertz dielectric properties of water measured with microwave microfluidic devices, *Rev. Sci. Instrum.* **81**, 054702 (2010).
[40]A. Baranyai and P. T. Kiss, Polarizable model of water with field-dependent polarization
, *J. Chem. Phys.* **135**, 234110 (2011).
[41]I. C. Yeh and M. L. Berkowitz, Ewald summation for systems with slab geometry, *J. Chem. Phys.* **111**, 3155 (1999).
[42]W. Shi and E. J. Maginn, Continuous fractional component monte carlo: An adaptive biasing method for open system atomistic simulations, *J. Chem. Theory Comput.* **3**, 1451 (2007).
[43]F. Moucka, M. Svoboda, and M. Lisal, Modelling aqueous solubility of sodium chloride in clays at thermodynamic conditions of hydraulic fracturing by molecular simulations, *Phys. Chem. Chem. Phys.* **19**, 16586 (2017).
[44]F. Moucka, M. Lisal, J. Skvor, J. Jirsak, I. Nezbeda, and W. R. Smith, Molecular simulation of aqueous electrolyte solubility. 2. Osmotic ensemble monte carlo methodology for free energy and solubility calculations and application to nacl, *J. Phys. Chem. B* **115**, 7849 (2011).
[45]F. Moucka, J. Kolafa, M. Lisal, and W. R. Smith, Chemical potentials of alkaline earth metal halide aqueous electrolytes and solubility of their hydrates by molecular simulation: Application to cacl2, antarcticite, and sinjarite, *J. Chem. Phys.* **148** (2018).
[46]F. Moucka and I. Nezbeda, Thermodynamics of supersaturated steam: Molecular simulation results, *J. Chem. Phys.* **145**, 244501 (2016).
[47]J. Chase, M., Thermochemical tables, *J. Phys. Chem. Ref. Monograph ACS, AIP* (1998).
[48]http://old.vscht.cz/fch/software/macsimus/.
[49]T. Darden, D. York, and L. Pedersen, Particle mesh ewald - an n.Log(n) method for ewald sums in large systems, *J. Chem. Phys.* **98**, 10089 (1993).
[50]I. F. W. Kuo and C. J. Mundy, An ab initio molecular dynamics study of the aqueous liquid-vapor interface, *Science* **303**, 658 (2004).
[51]M. D. Baer, C. J. Mundy, M. J. McGrath, I. F. W. Kuo, J. I. Siepmann, and D. J. Tobias, Re-examining the properties of the aqueous vapor-liquid interface using dispersion corrected density functional theory, *J. Chem. Phys.* **135** (2011).
[52]P. L. Silverstrelli and M. Parrinello, Water molecule dipole in the gas and in the liquid phase, *Phys. Rev. Lett.* **82**, 3308 (1999).
[53]P. Mark and L. Nilsson, Structure and dynamics of the tip3p , spc , and spc / e water models at 298 k, *J. Phys. Chem. A* **105**, 9954 (2001).
[54]R. K. Kalluri, D. Konatham, and A. Striolo, Aqueous nacl solutions within charged carbon-slit pores: Partition coefficients and density distributions from molecular dynamics simulations, *J. Phys. Chem. C* **115**, 13786 (2011).